Study on the Transmission and the Field Enhancement of Bi-Rhombic Aperture Arrays Structure

Xue Zhang, *Member, IEEE*, Shuzhan Yan, Jiahao Zeng, and Yun Fang, *Member, IEEE*

***Abstract*—This paper presents a new bi-rhombic aperture arrays structure (BAAs) that exhibits high transmission and extraordinary field enhancement. Through numerical simulation and theoretical analysis, the surface plasmon resonance mode and a quasi-FP resonance mode within the structure are approved to enhance the optical transmittance effectively. The transmission spectrum and the charge distribution of the resonance mode shows that the gap size and the bi-rhombic aperture short axis have a significant effect on shiftting of the spectrum without damping the transmission peak of the wave, enabling the achievement of both high transmission and high field enhancement. The optimized structure achieved a transmittance of 85% and a maximum enhancement factor of 18000. Besides that, an ultra-wide spectrum transmission in the near to mid-infrared was attained by adjusting the aperture structure. At wavelengths larger than mid-infrared, the transmittance can avoid damping, and the adjusted device is primarily sensitive to the lattice constant in one- direction. These results suggest that the proposed BAAs has significant potential for various applications in nanophononics, infrared sensing, and biomedical imaging.**

***Index Terms*—Surface plasmon resonance, field enhancement, extraordinary optical trasmission, quasi-FP resonance, surface-enhanced Raman scattering.**

I. Introduction

NANOSCALE hole apertures in a metallic film exhibit extraordinary optical transmission (EOT) [1], which led to their widespread use in modern optical technology, including optical filters, transparent electrodes in solar cells, flat panel displays, and light emitting diodes [2], [3], [4]. EOT in thin metal film nanoaperture arrays is mainly attributed to surface plasmon resonance (SPR) through surface plasmon polaritons (SPPs) and local surface plasmon resonance (LSPR) [5], [6], [7], [8], [9], as well as quasi-Fabry-Perot (FP) cavity resonance in longitudinal optical channels [10], [11], [12]. By manipulating different resonance modes, optical devices with diverse characteristics have been reported. Wang et al. achieved EOT and wide-spectrum transmission in near-infrared band by coupling SPPs and LSPR to an etched diamond-shaped aperture arrays on the Au film [8]. Zhang et al. excited the FP resonance mode by placing two metallic films and coupling it with surface plasma resonance to achieve high efficiency light transmission with a wide spectrum [13]. Shifting the transmission peaks of these devices often causes noticeable variations in both the peak value and bandwidth. In addition, it is also challenging to achieve both a significant enhancement factor and effective optical transmission simultaneously, as there is typically a trade-off between size and transmission efficiency.

Surface-enhanced Raman scattering (SERS) is a powerful technique for achieving remarkable local enhancement factors. This method involves the use of rough metal surfaces or nanostructures to amplify the Raman signal, resulting in greatly improved sensitivity and detection limits. SERS has numerous applications in fields such as biochemistry, environmental analysis, and materials science. In recent years, the quality of SERS substrates has considerably improved through the fabrication of plasmonic nanostructures, such as bow-tie [14], [15], [16], [17], island films [19], [20], nanowires [21], nanobundles [22], and nanocubes [23]. Plasmonic nanostructures have received particular attention since it would excite SPPs and create strong electromagnetic hot spots as well [24], [25], [26], [27], [28].

In this paper, we propose a bi-rhombic aperture arrays structure (BAAs), which is composed of a metallic silver film with a bi-rhombic aperture pattern etched on its surface and a lossless substrate. This device achieved the capabilities of EOT, as well as a significant field enhancement factor without sacrificing transmittance. By adjusting the short axis of the bi-rhombic aperture, we can effectively mitigate transmission intensity fluctuations and shift the peak value without compromising the overall transmittance. In addition, optical transmission in the near-middle infrared ultra-wide spectrum can be realized with a simple adjustment of the aperture structure. The characteristics of the device that is proposed in this paper are given in Section II. In Section III-A, how to realize both EOT and huge local enhancement factor is described in detail. In Section III-B, the extraordinary performance of ultrawide-spectrum transmission of the device is shown and analyzed.

Manuscript received 19 April 2023; accepted 26 April 2023. Date of publication 2 May 2023; date of current version 11 May 2023. This work was supported in by the National Natural Science Foundation of China under Grants 62101476 and 62201489, in part by the National Key Research and Development Program of China under Grant 2020YFA0713501, and in part by the Natural Science Foundation of Hunan Province of China under Grant 2022JJ40450. *(Corresponding author: Yun Fang.)*

The authors are with the School of Automation and Electronic Information, Xiangtan University, Xiangtan, Hunan 411105, China (e-mail: zhangxue.iecas@yahoo.com; szyan19990712@163.com; zjh@smail.xtu.edu.cn; fangyun@xtu.edu.cn).

Digital Object Identifier 10.1109/JPHOT.2023.3272340

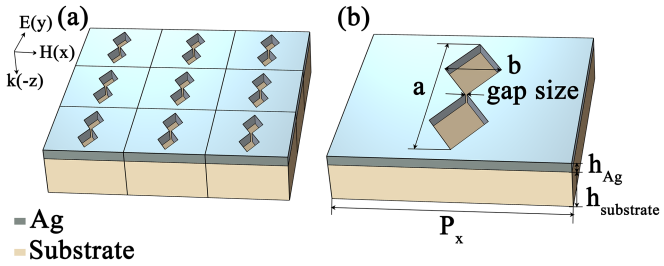

Fig. 1. Schematic of the designed BAAs structure and the corresponding cell structure of Ag BAAs on a binder substrate. A silver layer of 50 nm thickness is placed on an infinite substrate. The refractive index of the substrate is 1.5 in the NIR band range. ($P_x = P_y = 400$ nm, $g = 10$ nm, $a = 330$ nm, $b = 100$ nm).

II. Modeling

Fig. 1 depicts the structure of symmetric BAAs, etched in a 50 nm-thick nano-film of silver (Ag) with a refractive index of 1.5 in the near-infrared (NIR) band. The BAAs are positioned on an infinite substrate. The structure consists of diamond-shaped apertures with a length of long axis $a = 330$ nm and a short axis of $b = 100$ nm. The gap between the two tips of the bi-rhombic aperture structure was set to $g = 10$ nm. The arrays of structure has the period of $P_x = 400$ nm in the x-axis and 1.2 times the short axis a on the y-axis. The choice of silver as the construction material for BAAs was due to its low attenuation coefficient, and the material parameters were defined by the Drude model [29].

Numerical simulations were performed using the finite element method (FEM), with the incident light wavelength set to 1–2.5 um. The incident light's wavevector direction was perpendicular to the Ag film, and the direction of electric field polarization was parallel to the y-axis. Periodic boundary conditions were applied in the x and y directions, while a perfect match layer was set in the z direction. The transmittance of light can be obtained by the forward transmission coefficient S_{21}: $T(\omega) = |S_{21}|^2$, where $T(\omega)$ reprensents the transmittance.

III. Result and Discussion

A. EOT and Field Enhancement

To gain insights into the optical transmission properties of BAAs, a systematic investigation was conducted on the effects of various parameters such as the long axis a, short axis b, lattice period P_x, and gap size g on the spectra, as illustrated in Fig. 2(a)–(d). It was observed that an increase in the long axis a resulted in a slight enhancement of the transmission intensity and a broadened full width at half maximum (FWHM) with a red-shift of the transmission peak. While an increase in the short axis b from 100 nm to 300 nm could achieve an unattenuated shift of the transmission peak to the long-wave band due to a greater electron density at the gap arising from the diminution of the inclined angle. Comparatively, changes in the lattice period P_x not only cause a significant red-shift of the resonance peak, but also a reduction in both the intensity and FWHM of BAAs' spectra. This can be attributed to the substantial increase in the metal area within a single lattice. In contrast, we found out that changes in the period in the y direction had little effect on the

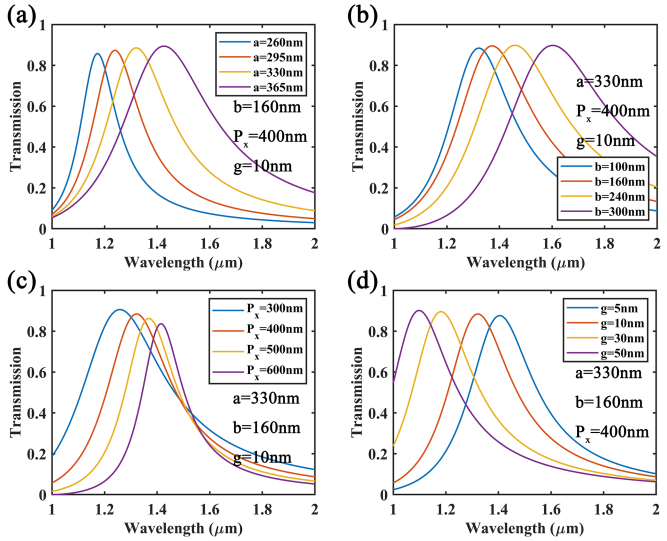

Fig. 2. Influence of different parameters on transmission spectrum, (a) bi-rhombic aperture long axis a increases from 260 nm to 365 nm, set b = 100 nm, $P_x = 400$ nm, $g = 10$ nm, (b) bi-rhombic aperture short axis b increases from 100 nm to 300 nm, set $a = 330$ nm, $P_x = 400$ nm, $g = 10$ nm, (c) period on the x-axes increases from 300 nm to 600 nm, set $a = 330$ nm, $b = 100$ nm, $g = 10$ nm, (d) gap size g of the bi-rhombic aperture increases from 5 nm to 50 nm,set $a = 330$ nm, $b = 100$ nm, $P_x = 400$ nm.

response of BAAs, indicating their relative insensitivity to such variations. Increasing the gap size g from 5 nm to 50 nm brought on a clear blue-shift in the resonance peak, as well as a trivial fluctuation in the transmission peak value and a broadnening of the FWHM, similar to the dimer structures [15], [26]. The shift of the transmission peak in this case was caused by changes in the inclined angle and tips' interaction, resulting in the damping of the electron density in the gap.

These results revealed that BAAs can achieve undamped shifts of ansmission peak and FWHM adjustments, with the short axis b of the bi-rhombic aperture proving to be a more effective adjustment parameter than the gap size commonly used in dimer structures. These findings offer valuable insights for the development of adjustable optical filters in the NIR band.

Building on our analysis of the impact of aperture parameters on the transmission spectrum, we extend our investigation to explore the correlation between structural parameters and transmission spectrum. The effective refraction index of the BAAs through S-paramenter inversion can be expressed as [30]:

$$n = \frac{1}{kt}\cos^{-1}\left[\frac{1}{2S_{21}}(1 - S_{11}^2 + S_{21}^2)\right] \quad (1)$$

Where, k, t, S_{21} and S_{11} are wavevector, sample thickness, transmission coefficient and reflection coefficient. Setting $P_x = P_y = 400$ nm, $g = 10$ nm, $a = 330$ nm, and $b = 100$ nm, the transmission spectrum and the effective refraction index of BAAs obtained is shown in Fig. 3. The effective refractive index is composed of both the real and imaginary parts, where the former represents the structure's dispersion to the electromagnetic wave and the latter represents its loss. The transmission peak occurs when the imaginary part of the effective refractive index approaches zero, indicating lower loss. When the incident

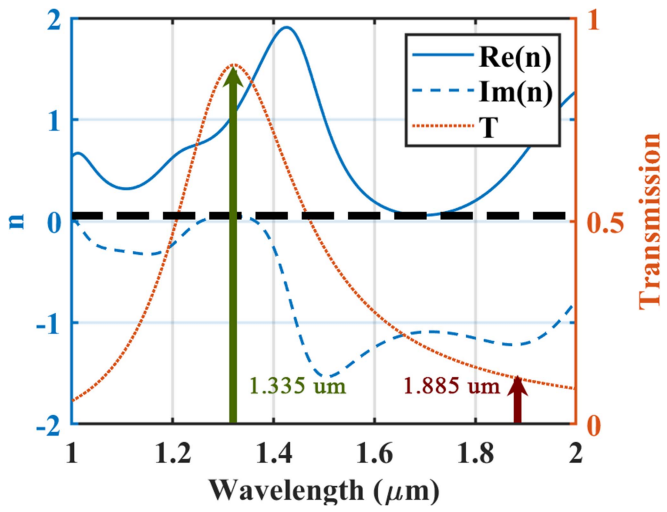

Fig. 3. Set $P_x = P_y = 400$ nm, $g = 10$ nm, $a = 330$ nm and $b = 100$ nm, transmission spectrum and effective refractive index.

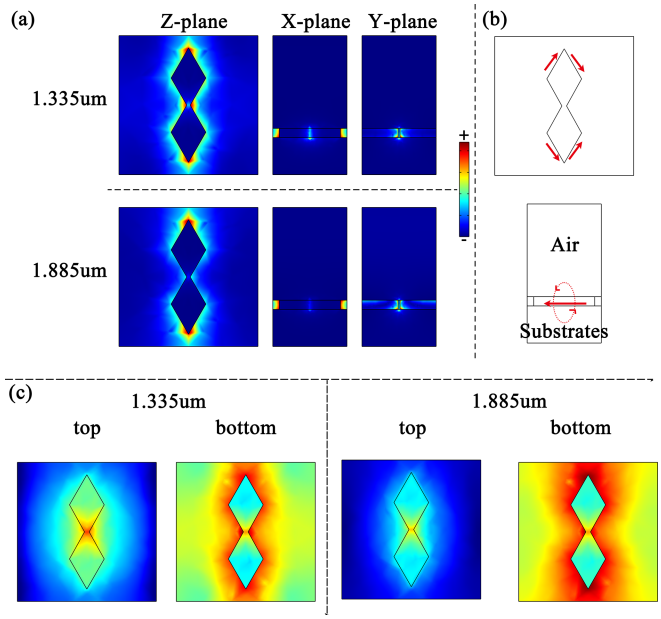

Fig. 4. When $P_x = 400$ nm, $g = 10$ nm, $a = 330$ nm and $b = 100$ nm, ((a) Charge distribution for an incident wavelength of 1.335 um (peak transmission) versus an incident wavelength of 1.885um (low transmission); (b) Induced current directions in the BAAs, XOY plane (upper panel), YOZ plane (lower panel), when the incident wavelength is 1.335 um (peak transmission); (c) aperture charge distribution (logarithmic) (intercepted from the Z-plane) with characteristic frequencies of 1.335 um (peak transmission) 1.885um (low transmission), respectively, including the upper surface of the silver film (left) as well as the lower one (right).

wavelength falls below the peak, the low real part of the effective refractive index causes reduced transmission efficiency, while above the peak, the high transmission loss impedes incident light from passing through the device.

To gain a deeper understanding of the physical mechanism underlying the transmission spectrum, we investigated the resonance principle of the device by analyzing the surface charge. Specifically, we computed the distribution of surface charges using the boundary values of electromagnetic field. In Fig. 4, we compare the resonance characteristics of incident light at two different wavelengths: 1.335 um, which corresponds to the peak transmission wavelength (indicated by the green line in Fig. 3), and 1.885 um, which corresponds to a wavelength of low transmission (also indicated by the red line in Fig. 3).

Fig. 4(a) displays a comparison of the charge density of the BAAs. At the peak transmission wavelength, the charge is predominantly concentrated around the bi-rhombic aperture in the z-plane, converging at the tip. In the x-plane, the similar distribution of charges is also observed across the metal tips, which proves the occurrence of SPR. This is the first resonant mode that supports the transmission spectrum. The distribution of charges in the metal film replicates the pattern of an FP cavity and is visible up and down in the y-plane. This phenomenon is known as a quasi-FP resonance, and it represents the second resonance mode of the transmission spectrum. It is worth noting that a similar charge distribution can be observed at the gap in the z and x planes. On the other hand, at $\lambda = 1.885$ um, the charges that are distributed up and down in the gap are reduced, which leads to a reduction in the quasi-FP resonance mode. While the charge in the rest regions, however, exerts trivial change. The weakening of the quasi-FP resonance mode is considered one of the reasons for the low transmission.

Thereafter, we give the direction of the induced current to prove the coexist of SPR and quasi-FP modes. Fig. 4(b) illustrates the direction of the induced current for the incident wavelength of 1.335 um. In the z-plane, the induced current in the aperture flows mainly around the perimeter of the aperture, consistent with the wrap-around distribution of charge. The current direction corresponds to the SPR mode as this dipole-charge oscillation is similar to that of nanoparticles at fundamental plasmonic resonances. In the X-plane, the induced current exhibits both horizontal motion along the metal layer, representing the SPR mode, as well as vertical motion through both the metal layer and the dielectric surface, representing the quasi-FP resonance mode.

In order to distinguish the roles of SPPs and LSPR in transmission spectrum, we intercepted the aperture of the structure from the z-plane and exhibited the charge distribution in Fig. 4(c). It can be seen that the charge distribution of the BAAs is influenced by the eigenmode in the bi-rhombic aperture and the lattice mode propagating between the periodic arrays. The intensity of LSPR affects the eigenmode, while the lattice mode is determined by the intensity of SPPs. At a wavelength of 1.885 μm, the higher charge density throughout the bottom metal layer significantly expands towards other lattice periods, suggesting the dominant influence of lattice modes between the periodic arrays on the transmission spectrum. Conversely, at a wavelength of 1.335 μm, dense charges appear at the aperture of the top metal layer, while sparse charges are present in the bottom metal layer, indicating an enhanced eigenmode and a weakened lattice mode.

To obtain an effective local electric field enhancement in BAAs, we adjusted the bi-rhombic aperture parameters and systematically studied the effect of aperture size and the lattice constant on the enhancement factor of electric field. We scanned the gap size g from 5 nm to 15 nm and studied the changes in the maximum field enhancement factor of the z-plane (the bottom surface of the metal film), as shown in Fig. 5(a). It is obvious that

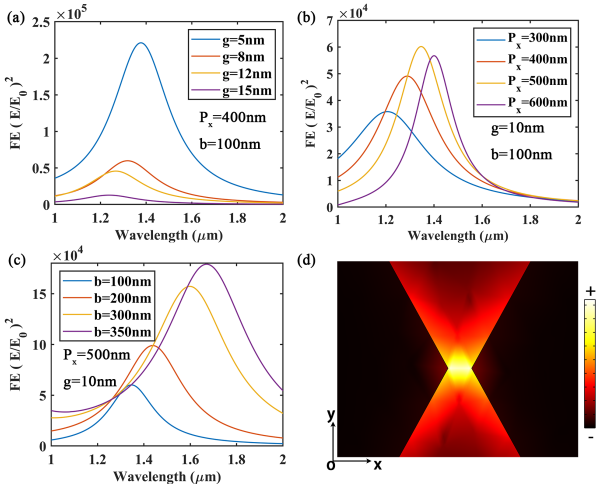

Fig. 5. Influence of different parameters on enhancement factor, set $a = 330$ nm, (a) gap size g of the bi-rhombic aperture increases from 5 nm to 50 nm, set $b = 100$ nm, $P_x = 400$ nm, (b) period on the x-axes increases from 300 nm to 600 nm, set $g = 10$ nm, $b = 100$ nm, (c) bi-rhombic aperture short axis b increases from 100 nm to 350 nm, set $g = 10$ nm, $P_x = 500$ nm, (d) electric field intensity of BAAs at the gap, set $g = 5$ nm, $P_x = 500$ nm, $b = 350$ nm.

adjusting the gap size g greatly affects the maximum enhancement factor due to the change in electronic density at the Raman tip, indicating the dominance of free electronic localization. The reduction in g corresponds to a decrease in the maximum field enhancement factor, suggesting the influence of SERS, which is also essential for the bi-rhombic aperture. However, limitations in the nano process preparation technology prevent us from reducing the gap size endlessly, making it necessary to explore alternative options to enhance the SERS tip effect.

In Fig. 5(b), we investigate the relationship between the lattice constant and the field enhancement factor. Although the lattice constant does not directly adjust the charge density of the Raman gap, a suitable P_x is conducive to the coupling of two Raman tips. Among the four sampling points in Fig. 5(b), 500 nm is the most appropriate lattice constant value. Additionally, Fig. 5(c) shows that b significantly affects the field enhancement factor due to the change in the inclined angle, which also affects the electronic density at the Raman tip. As mentioned earlier, b plays a similar role to g in the transmission spectrum, and adjusting them can shift the transmission peak. Therefore, the decrease of g and the increase of b can yield significant electric field enhancement while retaining good transmission efficiency. It should be noted that the transmission spectrum of the structure is compatible with its field enhancement spectrum, suggesting the advantageous impact of the EOT-induced free electronic oscillation on the SERS signal. Due to the small effect on the enhancement factor, the analysis of the bi-rhombic aperture's long axis a is not detailed here. Applying a group of optimized parameter, $g = 5$ nm, $P_x = 500$ nm, $b = 350$ nm, $a = 330$ nm, the distribution of the electric field at the gap is displayed in Fig. 5(d).

B. Near-Mid-Infrared Wideband Transmission Capability

Building on the previous research, adjustments were made to the aperture structure parameters, resulting in the improved

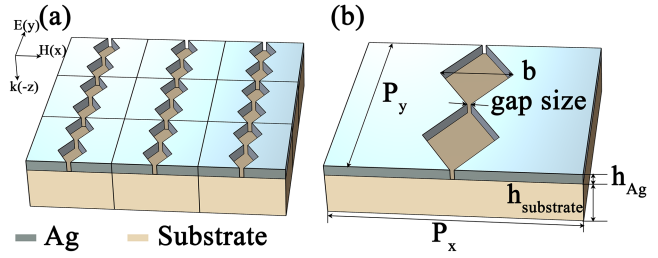

Fig. 6. Adjusted BAAs structure and the corresponding cell Structure of Ag BAAs on a binder substrate. A silver layer of 50 nm thickness is placed on an infinite substrate. The refractive index of the substrate is 1.5 in the NIR band range. ($P_x = 400$ nm, $g = 10$ nm, $P_y = 400$ nm, $b = 160$ nm).

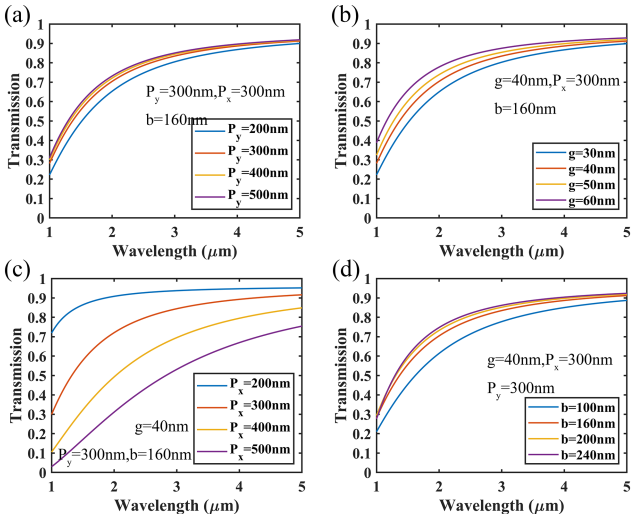

Fig. 7. Influence of different parameters on transmission spectrum, (a) period on the y-axes increases from 200 nm to 500 nm, set $g = 40$ nm, $P_x = 300$ nm, $b = 160$ nm, (b)gap size g of the aperture increases from 30 nm to 60 nm,set $P_y = 300$ nm, $g = 40$ nm, $b = 160$ nm, (c) period on the x-axes increases from 200 nm to 500 nm, set $P_y = 300$ nm, $g = 40$ nm, $b = 160$ nm, (d) short axis of the aperture b increase from 100 nm to 240 nm, set $P_y = 300$ nm, $g = 40$ nm, $P_x = 300$ nm.

BAAs shown in Fig. 6. We modify the long axis a to channelize the entire lattice along the z-axis. The material and dispersion characteristics remain the same as those studied above.

In order to make a depth understanding of the transmission behavior of the adjusted BAAs, we conducted an investigation of various parameters for the adjusted BAAs. The lattice period in the y-axis has a minimal effect on the transmission spectrum due to the lattice connection, as shown in Fig. 7(a). The optical transmission efficiency remains above 80% as the wavelength of the incident light increases. The transmittance almost avoids the influence of the gap size and the short axis, as depicted in Fig. 7(b) and (d). The inclined angle and electron density at the gap will alter because of changes to the short axis of the aperture and gap size, and this will produce a shift in the spectrum. In addition, when $b = 100$ nm, the weaker transmission spectrum is due to the small short axis length affecting the coupling between the eigenmode in the aperture and the lattice mode between the periodic arrays. As solely increasing the period of the lattice in the x-direction, the transmission spectrum has changed dramatically, as illustrated in Fig. 7(c). With the decrease of P_x, the transmission intensity increases significantly, which is due

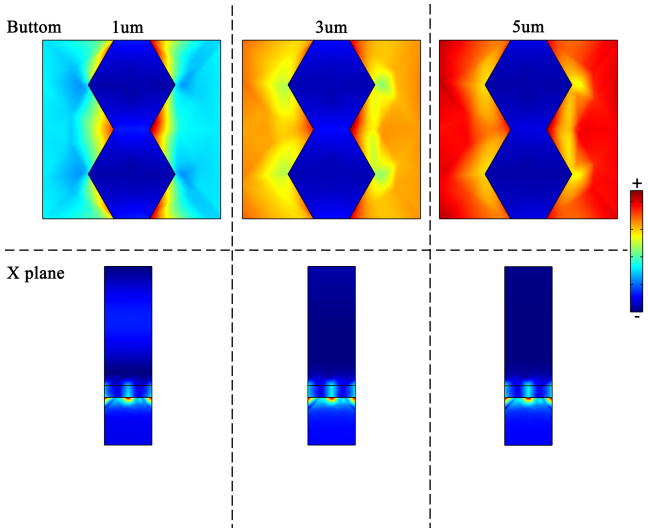

Fig. 8. Set $P_x = P_y = 300$ nm, $g = 40$ nm, $b = 160$ nm, charge density at the lower surface of the aperture and in the x-plane for incident light wavelengths of 1 um, 3 um, and 5 um.

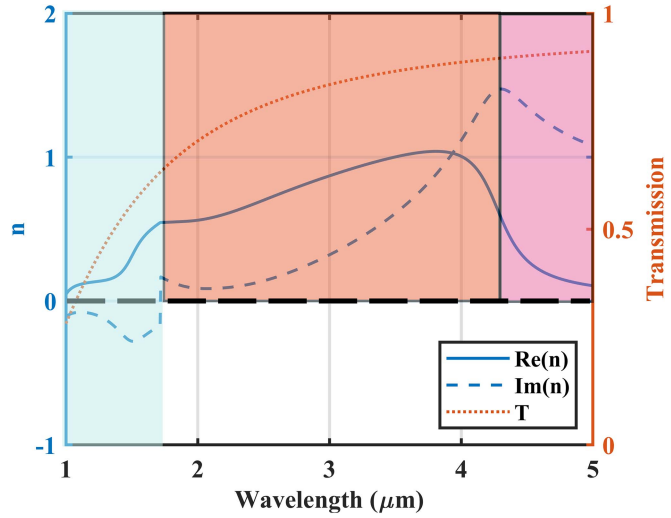

Fig. 9 Set $P_x = P_y = 300$ nm, $g = 40$ nm, and $b = 160$ nm, transmission spectrum and effective refractive index.

to the increase of the proportion of the aperture area in a lattice and the direct effect of P_x on the strength of the lattice mode. Besides, an overlarge P_x would interfere with the coupling of the eigenmode and the lattice mode,resulting in a great loss of transmission efficiency. Furthermore, transmission spectra with a larger incident wavelength range was calculated, and it was discovered that the structure's transmission efficiency does not damp. It is worth noting that the adjusted BAAs is not sensitive to structure parameters and the transmission spectrum exhibits excellent low-pass ability.

The resonant character of the adjusted BAAs is demonstrated by the charge distribution, which is given in Fig. 8 with the parameters $P_x = P_y = 300$ nm, $g = 40$ nm, $b = 160$ nm. It is obvious that the amount of charge in the aperture is negligible relative to that outside of the aperture, suggesting the domination of the lattice mode in this structure. As the incident light increases, the lattice mode gradually strengthens, as evidenced by the increase in charge density on the bottom surface. In addition, quasi-FP resonance mode is still present since the charges exhibit an up-and-down distribution in the x-plane at the gap. The charge distribution on the gap remains the same as the incident wavelength increases, demonstrating that the quasi-FP resonance does not decay as the wavelength of the incident light increases. It is suggested that the ultra-wide transmission spectrum is primarily guided by two resonance modes, including quasi-FP resonances and lattice modes in periodic arrays. As the wavelength of the incident light increases, the lattice mode becomes increasingly dominant, leading to broad-spectrum transmission. This structure can serve as a reference in designing filter components, such as efficient low-pass filters.

The modified BAAs exhibit a remarkable low-pass property that can be explained by analyzing their effective refractive index. In our analysis, we set $Px = P_y = 300$ nm, $g = 40$ nm, and $b = 160$ nm, and plotted the transmission spectrum and effective refractive index in Fig. 9. We divided the spectrum into three zones. In the blue zone, the effective refractive index has a negative imaginary part and a low real part, resulting in high loss and the low dispersion, which dampens the transmittance. As the wavelength increases, the lattice mode intensity improves, leading to an increase in the imaginary part of the effective refractive index in the orange zone. The increase in the imaginary part brings additional gain for the wave, which is also conducive to the wave transmission. Turning to the pink region, the lattice mode intensity tends to saturate, causing the imaginary part of the effective refractive index to decrease and the real part to go down as well. This leads to a steady state in the transmittance.

IV. Conclusion

In this study, we have developed a bi-rhombic aperture arrays structure that can achieve various functions with simple adjustments to its aperture parameters and period. Through the use of numerical simulation and optimization techniques, we were able to attain a substantial enhancement of the local field with a maximum factor of 18,000 in the near-infrared band. Furthermore, it was capable of shifting the transmission peak without damping the intensity while still maintaining over 85% of the transmission intensity. We demonstrated that the high enhancement factor did not compromise optical transmission efficiency. Additionally, our structure is capable of transmitting an ultra-wide spectrum in the near-mid-infrared band. These results suggest that the proposed BAAs has significant potential for various applications in nanophononics, infrared sensing, and biomedical imaging.

References

[1] T. W. Ebbesen, H. J. Lezec, H. F. Ghaemi, T. Thio, and P. A. Wolff, "Extraordinary optical transmission through sub-wavelength hole arrays," *Nature*, vol. 391, pp. 667–669, 1998.

[2] Z. L. Deng, Y. Cao, L X., and G. P. Wang, "Multifunctional metasurface: From extraordinary optical transmission to extraordinary optical diffraction in a single structure," *Photon. Res.*, vol. 6, pp. 443–450, 2018.

[3] A. M. M. Gherman, A. Vladescu, A. E. Kiss, and C. Farcau, "Extraordinary optical transmission through titanium nitride-coated microsphere lattice," *Photon. Nanostructures - Fundamentals Appl.*, vol. 38, 2019, Art. no. 100762.

[4] R. R. Ghosh and A. Dhawan, "Extremely large near-field enhancements in the vicinity of plasmonic nanoantennas on top of bull's eye structures exhibiting the extraordinary transmission of light," *OSA Commun.*, vol. 4, pp. 193–211, 2021.

[5] S. C. K. Goh et al., "Corner-promoted focus enhancement of light in conical holes for extraordinary optical transmission," *IEEE Sensors J.*, vol. 21, pp. 9081–9089, Apr. 2021.

[6] X. Zhang et al., "Tunable extraordinary optical transmission in a metal film perforated with two-level subwavelength cylindrical holes," *Plasmonics*, vol. 9, pp. 1149–1153, 2014.

[7] H. Q. Li, K. J. Wang, Z. G. Yang, and J. S. Liu, "Unexpected unidirectional perfect absorption of light in a freestanding optical thin metallic grating with extremely small filling factor," *J. Opt. Soc. Amer. B*, vol. 31, pp. 806–809, 2014.

[8] Y. K. Wang, Y. Qin, and Z. Y. Zhang, "Broadband extraordinary optical transmission through goad diamond-shaped nanohole arrays," *IEEE Photon. J.*, vol. 6, 2014, Art. no. 4801508.

[9] J. B. Pendry, L. Martin-Moreno, and F. J. Garcia-Vidal, "Mimicking surface plasmons with structured surfaces," *Science*, vol. 305, pp. 847–848, 2004.

[10] X. R. Huang, R. W. Peng, and R. H. Fan, "Making metals transparent for white light by spoof surface plasmons," *Phys. Rev. Lett.*, vol. 105, 2010, Art. no. 243901.

[11] S. Tajik and Z. Atlasbaf, "Investigating extraordinary optical transmission and sensing performance through periodic bilayer magneto-plasmonic structure," *J. Appl. Phys.*, vol. 127, 2020, Art. no. 023102.

[12] H. Q. Li, J. Liu, Z. Yang, and K. Wang, "High broadband transmission of light through a multi-layer sandwich microstructure containing a seamless metallic film," *IEEE. Photon. J.*, vol. 6, no. 5, Oct. 2014, Art. no. 4801807.

[13] S. Teeters-Kennedy et al., "Extraordinary infrared transmission of a stack of two metal micromeshes," *J. Phys. Chem. C.*, vol. 111, pp. 124–130, 2007.

[14] J. Park, H. Lee, A. Gliserin, A. Kim, and S. Kim, "Spectral shifting in extraordinary optical transmission by polarization-dependent surface plasmon coupling," *Plasmonics*, vol. 15, pp. 489–494, 2019, doi: 10.1007.s11486-019-01058-w.

[15] X. P. Zhu, S. Zhang, H. M. Shi, M. J. Zheng, and H. G. Duan, "Huge field enhancement and high transmittance enabled by terahertz bow-tie aperture arrays: A simulation study," *Opt. Exp.*, vol. 28, pp. 5851–5859, 2020.

[16] H. R. Park, X. Chen, N. C. Nguyen, J. Peraire, and S. H. Oh, "Nanogap-enhanced terahertz sensing of 1 nm thick (λ/106) dielectric films," *ACS Photon.*, vol. 2, pp. 417–424, 2015.

[17] H. R. Park et al., "Perfect extinction of terahertz waves in monolayer graphene over 2-nm-wide metallic apertures," *Adv. Opt. Mater.*, vol. 3, pp. 667–673, 2015.

[18] J. Langer, D. J. de Aberasturi, J. Aizupurua, and B. Zhao, "Present and future of surface-enhanced Raman scattering," *Aso. Nano*, vol. 14, pp. 28–117, 2019.

[19] P. F. Liao et al., "Surface-enhanced Raman scattering from microlithographic silver particle surfaces," *Chem. Phys. Lett.*, vol. 82, pp. 1–5, 1981.

[20] D. A. Weitz, S. Garoff, and T. J. Gramila, "Excitation spectra of surface-enhanced Raman scattering on silver-island films," *Opt. Lett.*, vol. 7, pp. 168–170, 1982.

[21] H. Dai et al., "Electricity mediated plasmonic tip engineering on single Ag nanowire for SERS," *Opt. Exp.*, vol. 26, pp. 25031–25036, 2018.

[22] S. J. Lee, A. R. Morrill, and M. Moskovits, "Hot spots in silver nanowire bundles for surface-enhanced Raman spectroscopy," *J. Amer. Chem. Soc.*, vol. 128, pp. 2200–2201, 2006.

[23] C. J. Orendorff, A. Gole, T. K. Sau, and C. J. Murphy, "Surface-enhanced Raman spectroscopy of self-assembled monolayers: Sandwich architecture and nanoparticle shape dependence," *Anal. Chem.*, vol. 77, pp. 3261–3266, 2005.

[24] G. F. S. Andrade, J. G. Hayashi, M. M. Rahman, W. J. Salcedo, C. M. B. Cordeiro, and A. G. Brolo, "Surface-enhanced resonance Raman scattering (SERRS) using Au nanohole arrays on optical fiber tips," *Plasmonics*, vol. 8, pp. 1113–1121, 2013.

[25] A. Mahigir, T. W. Chang, A. Behnam, G. L. Liu, M. R. Gartia, and G. Veronis, "Plasmonic nanohole array for enhancing the SERS signal of a single layer of graphene in water," *Sci. Rep.*, vol. 7, 2017, Art. no. 14044.

[26] H. Guo et al., "Optical resonances of bowtie slot antennas and their geometry and material dependence," *Opt. Exp.*, vol. 16, no. 11, pp. 7756–7766, 2008.

[27] M. Moridsadat and S. Golmohammadi, "Field enhancement in a terahertz plasmonic structure and it's sensing applications," in *Proc. Iranian Conf. . Elect. Eng.*, 2018, pp. 320–324.

[28] N. Gupta and A. Dhawan, "Bridged-bowtie and cross bridged-bowtie nanohole arrays as SERS substrates with hotspot tunability and multi-wavelength SERS response," *Opt. Exp.*, vol. 26, pp. 17899–17915, 2018.

[29] M. Ordal et al., "Optical properties of the metals Al, Co, Cu, Au, Fe, Pb, Ni, Pd, Pt, Ag, Ti, and W in the infrared and far infrared," *Appl. Opt.*, vol. 22, pp. 1099–1119, 1983.

[30] D. R. Smith, D. C. Vier, T. Koschny, and C. M. Soukoulis, "Electromagnetic parameter retrieval from inhomogeneous metamaterials," *Phys. Rev. E: Stat., Nonlinear, Soft Matter Phys.*, vol. 71, 2005, Art. no. 036617.